

## Photoinduced structural changes and related phenomena in amorphous arsenic chalcogenides

This article has been downloaded from IOPscience. Please scroll down to see the full text article.

1996 J. Phys.: Condens. Matter 8 429

(<http://iopscience.iop.org/0953-8984/8/4/009>)

[View the table of contents for this issue](#), or go to the [journal homepage](#) for more

Download details:

IP Address: 171.66.16.179

The article was downloaded on 13/05/2010 at 13:09

Please note that [terms and conditions apply](#).

# Photoinduced structural changes and related phenomena in amorphous arsenic chalcogenides

V I Mikla

Institute for Solid State Physics and Chemistry, Uzhgorod State University, Voloshina St. 54, 294000 Uzhgorod, Ukraine

Received 3 April 1995, in final form 15 August 1995

**Abstract.** The various photoinduced changes that occur in chalcogenide glasses upon absorption of band-gap light have been investigated by a variety of techniques. The first part of this paper describes studies by Raman scattering of the irreversible and reversible photostructural changes which occur in differently prepared vacuum-deposited amorphous chalcogenide films. Photoinduced changes in the Raman spectra in conventionally prepared amorphous  $\text{As}_2\text{S}_3$  films are interpreted by rearrangement of bonding configurations of molecular species which exist just after evaporation. The reversible photoinduced change in well annealed films involves a very small change in the short-range order. The most significant structural changes with photodarkening occur in the medium-range order. In the second part, the emphasis is placed on the light-induced changes in electrical transport properties. Several complementary experimental techniques have been employed including transient response, steady-state photoconductivity and xerographic measurements. Results suggest that metastable deep defect centres can be altered by irradiation. The observed changes in electronic transport are probably caused by the same photoinduced defects which give rise to the reversible photodarkening in a number of chalcogenide glasses.

## 1. Introduction

It is well known that for amorphous chalcogenide semiconductors some specific (unique) effects, not observable in its crystalline counterparts, are characteristic. Among these the photoinduced structural changes are the most intriguing [1–6]. At first sight, the phenomenon is simple and visual—under illumination with near-band-gap energy the transmittance of the samples substantially decreases and so-called photodarkening takes place. Such irradiation also causes a change in a wide variety of physical properties: rheological [7], physicochemical [8–11], optical [1–9], photoelectronic [12–14], etc. Photoinduced structural changes in amorphous chalcogenides may be divided into two categories: irreversible changes observed in as-deposited evaporated thin films, and reversible changes observed in well annealed thin films and melt-quenched glasses. In the latter case the change caused by illumination may be annealed out by heating at just below the glass transition temperature  $T_g$ . The change has recently received much attention because of its potential application for optical devices such as phase memories. Despite extensive study with various experimental probes, the nature and the mechanisms of photoinduced changes still pose an interesting open question in the physics of amorphous chalcogenides (for reviews of these phenomena see, for example, [2, 4–6].

The aim of the present paper is to investigate the light-induced changes in a local atomic structure and localized electronic gap states.

This paper is organized as follows. In section 2 a brief description of sample preparation and experimental methods is given. In section 3 we have examined the effect of the deposition, heat and light treatment on the structure of  $\text{As}_2\text{S}_3$  glass. Structural differences among films are discussed on the basis of the results of Raman scattering measurements. In section 4, photoinduced changes in electronic behaviour are described. In section 5, results are discussed phenomenologically and examined with respect to defect models. Finally, in section 6, we present the conclusions.

## 2. Experimental details

In order to investigate the origin of the changes under examination the Raman scattering spectra and electronic properties were studied. The majority of experiments were carried out on the model chalcogenide glasses  $\text{As}_2\text{S}_3$ ,  $\text{As}_2\text{Se}_3$  and Se.

The samples used in all studies were amorphous films typically 5–50  $\mu\text{m}$  thick and polished mirror-like plates of bulk glasses. The latter were prepared by the usual melt-quenching technique. Thin films were prepared by evaporating the bulk alloy powder from a molybdenum boat onto glass and quartz substrates at room temperature in a vacuum of  $10^{-6}$  Torr. The evaporation was performed under two different conditions: evaporation on a substrate held at  $T = 300$  K with a deposition rate of  $20 \text{ \AA s}^{-1}$  (conventional mode) and evaporation on a substrate held at  $T = 300$  K with a deposition rate of  $1 \mu\text{m s}^{-1}$  (flash evaporation).

Raman scattering was used to investigate structural changes in the samples. Right-angle Raman spectra were measured with the use of DFS-24 and RAMAMOR-U 1000 spectrometers with a classical photon-counting detection system. The spectral slit width was  $1 \text{ cm}^{-1}$  and the excitation wavelength was 633 nm. The polarization of the incident light was parallel to the scattering plane. Raman spectra of the amorphous films were recorded with sufficiently low incident laser beam power densities  $P = 3\text{--}5 \text{ mW}$  in order to avoid photostructural changes. The latter is known to transform the Raman spectra in a manner similar to that reported in [15] for amorphous selenium. The identity of the experimental spectra obtained from different points of the sample and the good reproducibility of the spectra in repeated scans show that photodarkening did not play a role in the subsequent Raman measurements.

The morphology of the films was analysed using a transmission electron microscope. For this purpose, the films were chemically removed from the substrates before examination. The results showed a clear amorphous structure for all the films examined.

The photoelectronic properties were examined via time-of-flight (TOF), xerographic and conventional (steady-state photocurrents and thermally stimulated currents (TSCs)) probes. For drift mobility measurements, films of thickness greater than 5  $\mu\text{m}$  were prepared by thermal evaporation of the bulk alloy onto glass substrates equipped with evaporated Au (or deposited  $\text{SnO}_2$ ) electrodes. The top sides of the samples were provided with semitransparent Au contacts by vacuum evaporation, forming sandwich configurations. The drift mobility of holes (electrons) was measured by the TOF method [16, 17]. Excess charge carriers were generated with a pulsed nitrogen laser. The light intensity was kept low in order to minimize the perturbing influence of trapped space charge. A DC electric field was applied a few seconds prior to the light pulse. The transient current was amplified and displayed on a storage oscilloscope. All TOF measurements were performed in the current mode in which case the time constant of the external circuit was kept short compared to the transit time. When dispersion entirely masks the transit time cusp, we define a statistical transit time from a double-logarithmic plot of the algebraically decaying current.

Two types of newly developed [18, 19] xerographic measurement also will be discussed, namely dark decay and cycled-up xerographic residual voltage. The former experiments were carried out by charging the surface of the sample from a corotron device and measuring the surface potential under an electrostatic probe. In the latter experiments (cycled-up residual voltage) the surface voltage following photodischarge in the xerographic cycle was monitored as a function of the number of cycles.

Band-gap illumination was provided by a mercury lamp, a He-Ne laser and Ar-ion laser. Except where noted, all the measurements were carried out at room temperature.

### 3. Photoinduced structural changes studied by Raman scattering

#### 3.1. Irreversible structural change

Photoinduced effects have usually been observed in thin film species of chalcogenide alloys [1-8]. These may be produced by the vapour deposition technique. In many cases, however, the initial structure of thin films is very different from that of well annealed films or bulk-glass counterparts and undergoes irreversible structural change in response to band-gap illumination or annealing. In order to elucidate the correlation between photodarkening and structure of amorphous semiconductors, we carefully examined the effect of preparation conditions and various treatments on the structure of  $As_xS_{1-x}$  films. The latter are particularly suitable for such a study because the irreversible changes in the optical properties in these materials are much more pronounced than in other chalcogenide glasses, e.g. in  $As_xSe_{1-x}$  [1-3, 20, 21]. The additional reason why these materials were selected is that relatively they hardly crystallize, thus permitting a wide range of preparation conditions [22].

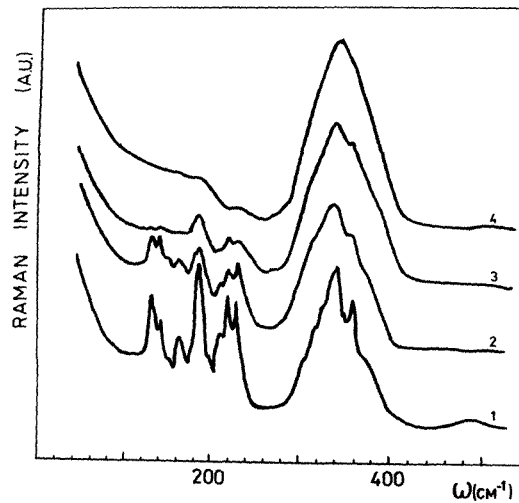


**Figure 1.** Raman spectra of an as-deposited (curve 1), a photodarkened (curve 2) and an annealed (curve 3)  $As_2S_3$  thin film, together with the Raman spectrum for a bulk glass of composition  $As_2S_3$  (curve 4) (a.u., arbitrary units).

Figure 1 shows the Raman spectra for the as-deposited (curve 1), exposed (curve 2), annealed film (curve 3) and bulk-glass (curve 4) forms of  $As_2S_3$ . Qualitatively similar

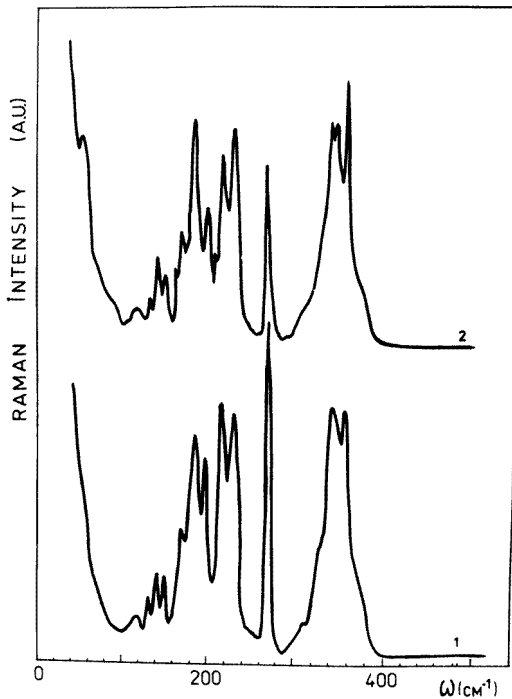


**Figure 2.** Raman spectra of a rapidly deposited  $\text{As}_2\text{S}_3$  film (a.u., arbitrary units). curve 1, spectrum prior to annealing; curve 2, spectrum of the annealed film.

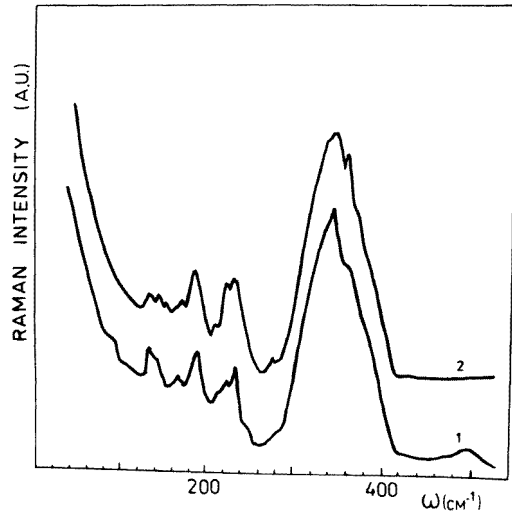


**Figure 3.** Raman spectra of films of composition  $\text{As}_{0.30}\text{S}_{0.70}$  (a.u., arbitrary units): curve 1, spectrum of a film prepared in a conventional manner (slowly deposited film); curve 2, spectrum of a rapidly deposited (flash evaporation) film.

results for irreversible thermostructural transformation have been reported by Solin and

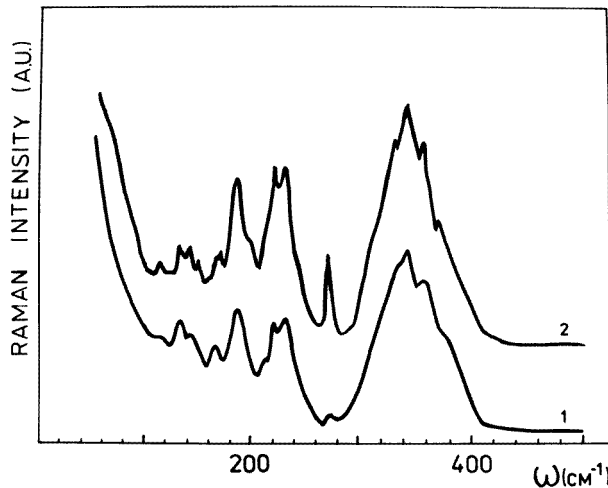


**Figure 4.** Raman spectra of  $\text{As}_{0.44}\text{S}_{0.56}$  films prepared by slow (curve 1) and fast (curve 2) evaporation (a.u., arbitrary units).

Papatheodoru [23] and Nemanich *et al* [24]. The spectrum of the as-deposited film consists of relatively sharp peaks superposed on a continual background of bulk  $\text{As}_2\text{S}_3$ . These sharp features of the as-deposited film broaden, decrease or disappear irreversibly, after annealing or illumination, indicating that significant structural modification takes place. Note that in As-rich glasses and amorphous films all these features are also observed. The characteristic sharp features in the region  $100\text{--}250\text{ cm}^{-1}$  have been assigned to molecular units such as  $\text{As}_4\text{S}_4$  and  $\text{S}_n$  [20, 23–26]. The presence of  $\text{As}_4\text{S}_4$  molecules in the as-deposited films is strongly supported by IR [27, 28] and EXAFS [29] measurements. Taking the above-mentioned facts into account, as-deposited films of  $\text{As}_2\text{S}_3$  possess  $\text{AsS}_3$  pyramidal units in addition to a partially polymerized mixture of  $\text{As}_4\text{S}_4$  (realgar type) and  $\text{S}_2$  and  $\text{S}_n$  molecular species.

After annealing, the as-deposited film spectrum becomes very close to that of bulk glass except for some remaining bending bands of As–As vibration, indicating the presence of a small amount (few per cent in accordance with [24]) of  $\text{As}_4\text{S}_4$  molecules. During this treatment the bond breaking and switching due to increased mobility of atoms are accompanied (to a considerable extent) by structure polymerization. This was manifested in the S–As–S stretching mode ( $120\text{--}170\text{ cm}^{-1}$ ), frequency spreading and vibrational band broadening so typical of a bulk glass. A similar behaviour in the valence mode region of As–S and As–As vibration bands takes place if we illuminate the as-deposited film. However, in this case the S–As–S mode broadening is very slight. Consequently, illumination causes the structure of the as-deposited films to become closer to the network structure of the bulk. Note that for the Se-based compositions the difference between the spectra of melt-quenched glassy and freshly deposited samples is not so dramatic as in the case of the As–S system.

It is not surprising that amorphous sample properties can depend (sometimes critically) on the parameters of the preparation process<sup>†</sup>. This is because of the ability of amorphous structure to realize one of possible and appropriate metastable structural configurations. The

<sup>†</sup> Nevertheless, most of the available experimental data show [3, 6] that the fundamental characteristics of photodarkening are not affected by variations in the preparation technique for the sample. Only in [31] has it been reported that the quenching temperature may have some influence on the photodarkening of bulk glasses.

above-mentioned results correspond to samples produced in a conventional manner. The reaction of these samples on band-gap illumination is manifested in an absorption edge shift to lower energies ('red' shift or photodarkening). By analogy with silver halide photographic materials we refer to such samples as 'negative'. In contrast, exploiting a special kind of evaporator ( $T_{evap} = 800\text{--}900\text{ }^{\circ}\text{C}$ ; deposition rate,  $1\text{ }\mu\text{m s}^{-1}$  or more), described in [30], leads to structural modification which in turn results in a decrease in the optical band gap. The samples being exposed behave like 'positive' photosensitive materials, i.e. possess a shift of absorption edge to a position higher in energy (photobleaching).

In figure 2, a typical Raman spectrum of rapidly deposited ('positive') film is shown. In general, it is clear that on raising the evaporation temperature and deposition rate the spectral bands sharpen and the continuum background disappears. The high-frequency component at  $490\text{ cm}^{-1}$  which represents S-S bonds polymerized in a glass network also disappears. This is paralleled by the appearance of additional features at 120, 150, 200, 233 and  $273\text{ cm}^{-1}$ . Note that the strongest peak ( $272\text{ cm}^{-1}$ ) in the Raman spectrum of the film deposited at a high deposition rate is absent in those of  $\text{As}_2\text{S}_3$  crystals and  $\alpha\text{-As}_4\text{S}_4$  and  $\beta\text{-As}_4\text{S}_4$  polymorphs. Recall that this line was observed [32] in the Raman spectrum of sample of crystalline  $\text{As}_4\text{S}_3$  obtained by vacuum sublimation of a melted sample of  $\text{As}_4\text{S}_3$  composition.

However the films were found to become sulphur deficient as the deposition rate is increased. This is the case even for sulphur-rich compositions (figure 3). One of the reasons for such an As enrichment of the samples may be partial fragmentation of  $\text{As}_2\text{S}_3$  into  $\text{As}_2\text{S}_2$  and sulphur during the deposition. Note that an increase in the quenching temperature has a similar effect on the structure of melt-quenched  $\text{As}_2\text{S}_3$  as was demonstrated by Yang *et al* [33] and Mikla *et al* [34].

Only a slight change in the Raman spectrum after irradiation of such films is observed. On the contrary, annealing results in further narrowing of the bands, their splitting and intensity redistribution. The low-frequency region of an annealed film exhibits a distinct shoulder at about  $60\text{ cm}^{-1}$  which probably corresponds to the lattice line in the spectra of the crystals  $\alpha$ ,  $\beta\text{-As}_4\text{S}_4$  [26].

What is important to point out here is that the transformation of the Raman spectrum with increasing As content (above stoichiometric composition) is similar to that observed in  $\text{As}_2\text{S}_3$  with increasing deposition rate (for comparison see figures 2 and 4). The results suggests that the high deposition rate induces the development of the tendency to microcrystallite formation. A further anneal enhances the crystallization processes and the films became polycrystalline. Such a radical structural transformation, observed in films deposited at high rates and was found to be irreversible; the initial structure (and the corresponding absorption edge position) could not be restored even by annealing at temperatures  $T \simeq T_g$ . Moreover, the 'positive' films which initially always appeared smooth took on a 'dusty' appearance after light and especially heat treatment. This is probably caused by  $\text{As}_2\text{O}_3$  crystals which are formed when the films are illuminated or heated in air.

### 3.2. Reversible structural change

Returning to the films prepared in conventional mode (negative), we next examine how the photodarkening of well annealed films and bulk samples (i.e. reversible photodarkening) influences their structure. This is much less pronounced than for the irreversible changes discussed above, principally because the size of the reversible photodarkening effect is small. Structural changes detected by means of direct structural probes (e.g. x-ray diffraction [35]) are subtle. At the same time, Raman scattering is believed to be sensitive to the above-

mentioned effects. Frumar *et al* [36] reported an increase in the intensity of the  $231\text{ cm}^{-1}$  Raman band characteristic of As–As bonds in a-As<sub>2</sub>S<sub>3</sub> with photodarkening. In contrast, in the present experiments no slight change in Raman spectra in the frequency range  $100\text{--}500\text{ cm}^{-1}$  could be detected. Only low-frequency Raman spectra show [37–39] discernible changes under illumination.

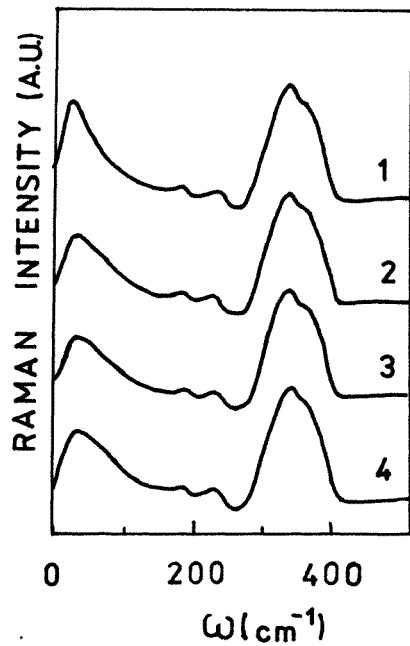


**Figure 5.** Evolution of the Raman spectra in glassy samples of As<sub>2</sub>S<sub>3</sub> exposed to laser irradiation at 514 nm (a.u., arbitrary units): curve 1, reference spectrum of glassy state; curves 2, 3 and 4, after 3 min, 5 min, and 7 min exposure, respectively to  $10^2\text{ W cm}^{-2}$ . All spectra were normalized to the height of the  $340\text{ cm}^{-1}$  Raman band.

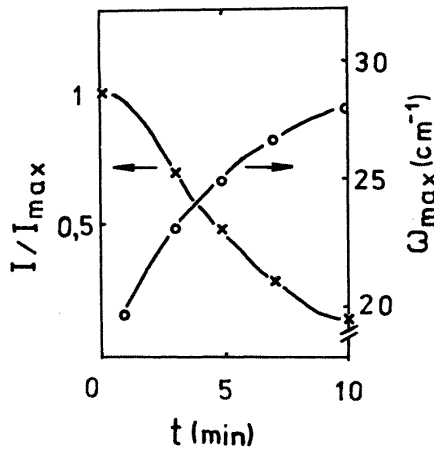


**Figure 6.** The low-frequency peak position and relative intensity as a function of exposure time.  $I_{\max}$  denotes the peak intensity for a non-darkened sample.

In figure 5, the Raman spectra measured at room temperature are shown. As<sub>2</sub>S<sub>3</sub> glassy samples were illuminated at various times from 1 to 20 min. It is observed that the low-frequency peak position of the spectrum gradually shifts to higher frequencies as the illumination time is increased. The reversible photodarkening in As<sub>2</sub>S<sub>3</sub> annealed thin films and bulk glasses is accompanied also by changes in the intensity of low-frequency peak (figure 6). It is clear that the photodarkening has reduced appreciably the intensity of so-called boson peak.

In the subsequent part of this paper, the focus is on reversible photoinduced effects. Data will be presented for As<sub>x</sub>Se<sub>1-x</sub> only but qualitatively similar (although less pronounced) effects are observed for As<sub>x</sub>S<sub>1-x</sub> alloys. The reason why we focus the study of photoinduced electronic effects on Se-based alloys is that certain experimental limitations seem comparatively smaller for these materials. For example, amorphous As<sub>x</sub>Se<sub>1-x</sub> alloys with  $0 \leq x \leq 0.20$  are particularly suitable for studying electron transport processes because of their ambipolarity.

#### 4. Photoinduced electronic effects

##### 4.1. Steady-state photocurrents

There is strong evidence to suggest that most of the reported photoinduced optical and structural changes affect the band-gap states. Several research groups have devoted considerable efforts to experiments which probe the gap states near mobility edges and within the mobility gap [8, 12–14, 18, 19, 39–42]. This is not an easy matter; no single experiment gives complete and unequivocal information and obviously it is necessary to bring together data from a wide range of measurements, stationary as well as transient.

First of all we consider the associated changes in the photoelectronic properties of the samples. The spectral characteristics of photoconductivity of the samples display a red shift after irradiation. Such behaviour of the photoconductivity is not surprising, as it is in full agreement with the shift in the absorption edge. Additionally, the photoconductivity decreases after photodarkening. The decrease may be attributed to the creation of new defect localized states.

Lux–ampere characteristics for annealed films are characterized by a sublinear dependence  $I_{ph} \sim E^n$  in a wide light intensity range,  $n$  being equal approximately to 0.6 for  $\text{As}_2\text{Se}_3$ . After darkening, the index  $n$  increases.

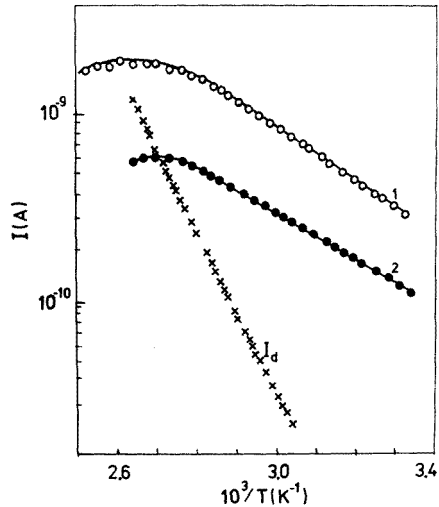


**Figure 7.** Steady-state photocurrent from an a- $\text{As}_2\text{Se}_3$  sample for 700 nm illumination with approximate intensity of  $10^{14}$  photons  $\text{cm}^{-2} \text{ s}^{-1}$  as a function of inverse temperature (curve 1). Also shown is the effect induced by laser irradiation ( $\lambda = 633$  nm) at  $T = 100$  K (curve 2).

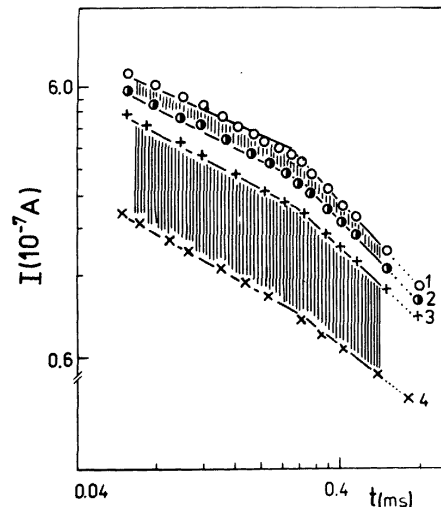


**Figure 8.** Transient hole current (from TOF measurements) in a- $\text{As}_2\text{Se}_3$  ( $d = 3.4 \mu\text{m}$ ;  $E = 5.3 \text{ V } \mu\text{m}^{-1}$ ;  $T = 293$  K): data 1 and 2, annealed sample; data 3 and 4, photodarkened sample. The areas between data 1 and 2 and between data 3 and 4 indicate space-charge accumulation during a ten-transit sequence with a repetition frequency of 10 Hz.

The temperature dependence of the steady-state photocurrent is generally quite similar to those observed widely [43–45] in chalcogenides. Figure 7 shows that photoconductivity is an activated process and varies exponentially with  $1/T$ . The activation energy from the plots of  $\log I_{ph}$  versus  $10^3/T$  turns out to be 0.31 eV. Also plotted in the figure is the variation in dark conductivity with temperature, which is also an activated process.

Since it is generally accepted [45] that in chalcogenide semiconductors recombination will be mediated by the charged defect states, we may analyse the temperature dependence of the steady-state photocurrent in terms of an energy scheme involving acceptor-like levels in the gap. It has been shown [45] that the low-temperature 'bimolecular' slope  $\Delta E_b$  represents half the distance between the valence band and acceptor-like level. The observed differences in  $\Delta E_b$  with exposure ( $\Delta E_b \simeq 0.22$  eV in irradiated samples) therefore indicate that illumination influences the gap-state density in the lower half of the band gap.

The above changes in the photocurrent of amorphous chalcogenides may be related to specific changes in electronic gap states, which act as trapping and recombination centres and which therefore limit the photoconductivity.

#### 4.2. Light-induced effects on photocurrent transients

Currently two classes of transient photocurrent experiments can be distinguished. On the one hand, there is the unipolar method. The most common is the TOF experiment developed by Spear [16]. In the TOF method the carriers are created near one electrode of a sandwich configuration. This configuration makes it possible to distinguish electron and hole motion. The carrier mobility is determined by the position of the break in the current pulse. Therefore, the precise knowledge of concentration of the transiting carriers is not necessary. To observe the transit pulse in the TOF experiment, the electrode must form a blocking contact, i.e. must be unable to inject carriers. To prevent distortion of the field, the excess charge introduced should be less than  $CV$ , where  $C$  is the capacitance of the sample and  $V$  is the voltage across the sample.

On the other hand, there is the bipolar measurement of the transient photocurrent due to electrons and holes in the gap-cell configuration [42]. In these experiments the sample is illuminated uniformly in the direction transverse to the electrodes, creating an excess conductance  $G$ . Injecting contacts supply the excess current  $I_{ph} = GV$  for a bias voltage  $V$ . There is no build-up of charge at the electrodes. Furthermore, the excited region between the contact remains electrically neutral. As a result, signal averaging with repetitive pulses is easy. When analysing coplanar transient photocurrents, the different drift mobilities of electrons and holes, together with the recombination, must be taken into account.

Figure 8 reproduces the major results of extensive experimental studies on hole transport in a-As<sub>2</sub>Se<sub>3</sub>. The current traces are shown as  $\log I$  versus  $\log t$  for constant field and constant temperature. Just after irradiation a drastic change in transient photocurrent was observed;  $I_{ph}$  decreased in magnitude, and the slope of transient also changed.

The shape of the transient hole current in dark-rested samples is typically dispersive and exhibits two distinct algebraic time dependences. From the data obtained, it is obvious that the transit time  $t_T$  (identified by the intercept of the respective straight lines in the double-logarithmic plot) remains unchanged by photodarkening [14]. Here it is necessary to note that, for samples photodarkened to saturation, the  $\log I$  versus  $\log t$  plot yielded a straight line from which no transit time could be extracted. In this case, only a lifetime-limited signal is observed.

As can be seen from figure 8, the dispersion of the transit pulse tends to increase with photodarkening. In fact, the initial (pre-transit) current slope increased whereas the final (post-transit) current slope decreased. The important result of this experiment is the observation that the hole drift mobilities  $E_\mu^h$  are the same before and after light exposure. A similar behaviour has been detected in mobility measurements on a number of other disordered chalcogenides. Subsequent annealing restores the initial state.

Drift mobility experiments may be affected by [16] two kinds of space charge effect.

First of all, it is the presence of deep centres in the gap. These centres gradually accumulate charge with each drift pulse, especially near the surfaces of a specimen, which leads to a decreasing internal field. As a result the transient current decreases in magnitude. Secondly, at high photoinjection levels ( $Q > CV$ , where  $C$  is the sample capacitance and  $V$  is the applied field), space charge may be formed by the drifting packet itself. In our case this latter can be excluded because of the small value of injected charge ( $Q \leq 0.1CV$ ). A space charge effect of the former kind is illustrated in figure 8. It is obvious that band-gap light leads to the development of a pronounced variation in the space charge in the sample. The estimated amount of charge accumulated by deep traps during a ten-transit sequence increases 1.3–2 times at least at photodarkening and approaches approximately  $10^{14} \text{ cm}^{-3}$ .

Consequently, shallow states which control charge transport and define the activation energy  $E_\mu^h$  (about 0.4 eV for  $\text{As}_2\text{Se}_3$ ) of the mobility should not undergo photoinduced changes. At the same time it should be stressed that the observed change in the current transient (namely its increased dispersion and decreased magnitude) indicate photoinduced changes of deep states with  $E_i > E_\mu^h$ . Such behaviour is probably related to enhanced carrier trapping by deep levels in photodarkened samples.

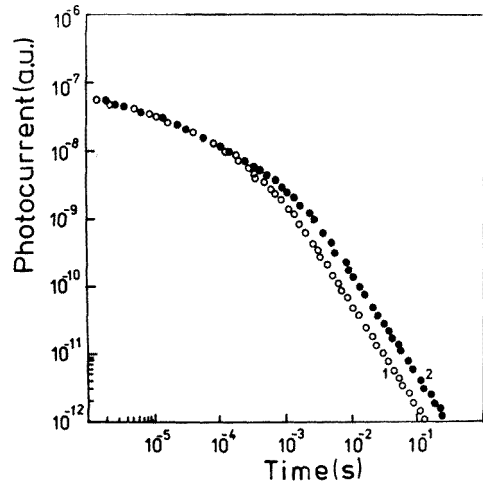


**Figure 9.** The transient photocurrent from fully annealed (data 1) and photodarkened (data 2) a- $\text{As}_2\text{Se}_3$  gap cells after flash excitation ( $\lambda_e = 690 \text{ nm}$ ) (a.u., arbitrary units). The data are normalized at the earliest time for ease of comparison. The change in slope of the photocurrent transients is identified as  $\tau_{MR}$ .

Next, we turn our attention to the monomolecular recombination process which appears in the photocurrent transients in figure 9. This plot of  $\log I$  versus  $\log t$  compares the transients for non-photodarkened and photodarkened samples. The behaviour of the photocurrent is seen to be very similar to that of the current in the TOF experiment. In both cases the photocurrent makes a sharp transition from a power law with exponent less than one to a power law with exponent greater than one (compare curve 1, figure 8, with curve 1, figure 9). Clearly, the monomolecular recombination time  $\tau_{MR}$  plays the same role in the photocurrent experiment that the transit time  $t_T$  plays in the TOF experiment. In fact, Orenstein and Kastner [42] assumed that the photocurrent would decay this way.

As is clear from figure 9,  $\tau_{MR}$  is slightly dependent on the light treatment. In principle,

the carrier lifetimes are given by the formula

$$\tau_{MR} \sim 1/v_0(b_t N_L/b_r N_{th})^{1/\alpha}$$

where  $v_0$  is the pre-factor of the release rate from localized states (typically of the order of  $10^{12}$ – $10^{13}$  s $^{-1}$ ),  $b_t$  is the trapping coefficient,  $N_L$  is the factor of the density of localized states,  $b_r$  is the recombination coefficient,  $N_{th}$  is the thermal equilibrium concentration (of recombination centres) and  $\alpha$  is the dispersion parameter characteristic of anomalous charge transport. There are two factors which both tend to make  $\tau_{MR}$  greater as the sample is photodarkened. The first is the trap-limited mobility and the second is the concentration of recombination centres. From TOF data, the mobility remains unchanged with photodarkening. That is why we speculate that the change in  $\tau_{MR}$  can be explained by the second factor alone.

#### 4.3. Non-isothermal relaxation of low-temperature photoinduced effects

A durable photoinduced change known as photodarkening is retained unless the sample is annealed. In addition to this permanent change, transient (dynamical) photoinduced changes have also been observed in chalcogenide glasses [46, 47]. There are some indications [39] that the dynamical changes are probably due to an alteration of metastable defects which act as shallow traps for carriers generated by band-gap light. Reasonably, one can expect that the non-equilibrium carriers become immobilized for a long time in these states if the irradiation temperature is essentially lowered. In an earlier publication [20, 40] it is assumed that the magnitude of photodarkening is increased at low temperatures due to the additional (with respect to room-temperature) component. The latter manifests itself as dynamical changes in transmissively and refractive index at room temperature whereas it is transformed to a permanent change at  $T = 100$  K. That is why it seemed plausible to study the non-isothermal relaxation of the low-temperature photoinduced effects.

Several transient and/or stationary methods may be properly employed in studying electronic and atomic relaxation. For this purpose, TSCs and holographic grating techniques were used. The latter can monitor even small changes in refractive index.

In the present investigation, a grating having a pitch  $\Lambda = \lambda_e/[2 \sin(\theta/2)]$  is produced at  $T = 100$  K by two interfering beams of wavelength  $\lambda_e$  ( $= 633$  nm), intersecting at a sample surface with an angle  $\theta$  ( $\sim 40^\circ$ ). The diffraction efficiency  $\eta = I/I_0$ , where  $I_0$  and  $I$  are the corresponding intensities of the reading beam and of the first-order diffracted beam, is measured as a function of rising temperature. The reading beam of wavelength  $\lambda_r$  ( $= 900$  nm) emitted by a 10 mW GaAs laser appears to be little affected by a change in absorption coefficient with rising temperature.

Figure 10 shows the typical response of light intensities diffracted from gratings formed on an  $\text{As}_{0.5}\text{Se}_{0.5}$  film. The  $\eta$  versus  $T$  data exhibit several stages: an initial invariance followed by a rapid increase at  $T = 200$  K and then decreasing to values of  $\eta/\eta_{max} = 0.3$  at  $T = 300$  K. Finally, at  $T \geq 420$  K (this high-temperature region is not shown in figure 10),  $\eta$  falls to zero, and the grating is completely erased. Note that the relative increase in  $\eta$  observed when the temperature range 210–230 K is about 50% with respect to its value at  $T = 100$  K. This effect (namely ‘self-enhancement of holographic recording’) may be of practical importance because it permits the diffraction efficiency to be essentially increased without additional treatment such as substrate metallization and chemical etching. There are, however, factors limiting its applicability. Among them are the low-temperature holographic recording itself and inconveniences connected with such a procedure, a vanishingly small effect in a more suitable ( $T \geq 300$  K) temperature range.

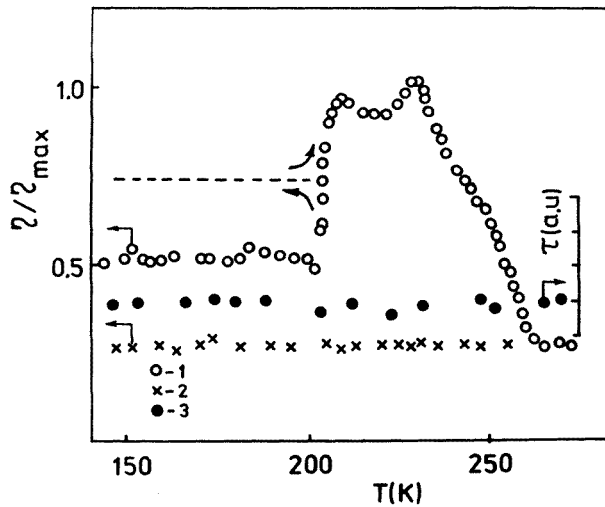


**Figure 10.** The diffracted light intensity from gratings formed on an  $\text{As}_{0.5}\text{Se}_{0.5}$  thin film at  $T = 100$  K (data 1). Also shown is the  $\eta$  versus  $T$  dependence after annealing at  $T = 300$  K (data 2) (a.u., arbitrary units). Note that the transmissivity of a fully annealed film is nearly temperature independent at  $\lambda_r = 900$  nm (data 3).

Now we turn our attention to data on TSCs. In order to be able to find correspondence to data on gratings, TSC measurements were performed on identical samples. The latter were illuminated at  $T = 100$  K; the total exposure used was approximately the same as in the grating experiment. Figure 11 shows a well shaped TSC peak with  $T_{max} = 275$  K. The activation energy  $E_i$  associated with the peak has been calculated by the initial rise method [48]. The  $E_i$  value obtained by this method is about 0.4 eV.

With regard to  $\eta$  versus  $T$  and  $I_{TSC}$  versus  $T$  dependences, note only that there is a certain correspondence; when the trapped carriers in the gap states of  $E_i = 0.4$  eV were emitted with a temperature rise the diffraction efficiency distinctly decreases. At the same time, the thermal decays of the two effects differ at higher temperatures. The TSC indicates almost complete annealing but a substantial fraction of  $\eta$ , induced at  $T = 100$  K, is still present even at 300 K.

#### 4.4. Transient aspects of photoinduced effects

In a previous section we consider how the photoinduced effects can be annealed away. It is instructive now to examine the temporal behaviour of photoinduced changes. Pure amorphous selenium and  $\text{As}_x\text{Se}_{1-x}$  alloys with  $0 < x < 0.2$  seem to be extremely suitable objects for this purpose. On the other hand, at room temperature, they exhibit only transient (dynamical) photoinduced changes in optical properties. No permanent changes can be induced at  $T = 300$  K since the glass transition temperatures ( $T_g = 314$  K and 330 K for Se and  $\text{As}_{0.05}\text{Se}_{0.95}$ , respectively [22]) are close to the illumination temperature [16, 47]. The effect consists of a decrease (less than 8%) in transmission during illumination which is spontaneously restored as the excitation was switched off. On the other hand, relatively well defined drift mobilities for both holes and electrons are characteristic for the composition mentioned.

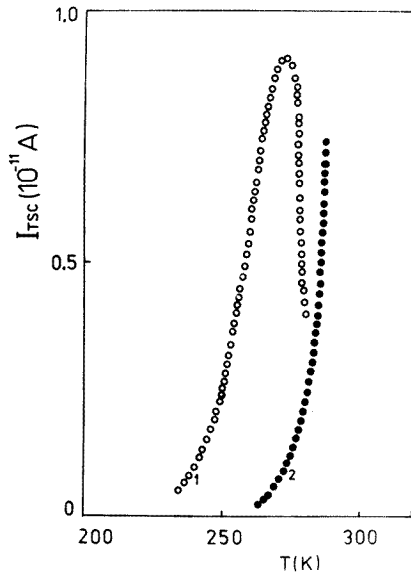


**Figure 11.** A TSC curve in a-As<sub>0.5</sub>Se<sub>0.5</sub> (data 1). The sample was cooled to 100 K and then exposed to laser illumination at 633 nm. After the whole TSC curve has been obtained, a second thermal cycle for an unexcited sample is started (data 2). As for figure 10, the heating rate is 0.1 K s<sup>-1</sup>.

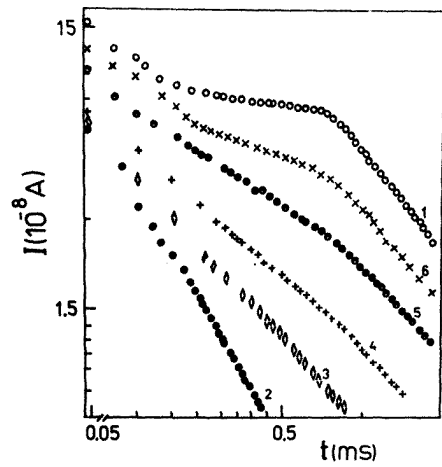


**Figure 12.** Transient electron current in a-As<sub>0.1</sub>Se<sub>0.9</sub> samples ( $d = 4.4 \mu\text{m}$ ;  $E = 3.7 \text{ eV } \mu\text{m}^{-1}$ ;  $T = 293 \text{ K}$ ): data 1, dark rested; data 2, exposed; data 3, 4, 5 and 6, exposed and then dark rested for 5 min, 10 min, 50 min and 160 min, respectively.

We consider first the effect of pre-illumination on carrier drift in As<sub>x</sub>Se<sub>1-x</sub> films. Figure 12 shows a typical trace of the transient electron current in dark-rested and pre-exposed As<sub>0.1</sub>Se<sub>0.9</sub> samples. It is apparent that pre-illumination leads not only to a decreasing magnitude of the photocurrent transient but also to an abrupt transformation of the signal character: from a pulse with well defined transit time (curve 1) to a featureless lifetime-limited pulse (curve 2). If, after pre-illumination, the film is allowed to relax in the dark, the previous (dark-rested) shape of the transient current is fully recovered, i.e. the pulse height and shape return to values characteristic of the unexposed sample. It is found that the charge carrier lifetime  $\tau_L$  with respect to deep trapping decreases approximately by an order of magnitude. For example  $\tau_L \leq 0.5 \text{ ms}$  for electrons in the previously illuminated sample As<sub>0.1</sub>Se<sub>0.9</sub>.

Figure 13 shows the relaxation function  $\Psi(\tau)$  for hole (electron) metastable traps in exposed As<sub>x</sub>Se<sub>1-x</sub> alloy films.  $\Psi(\tau)$  is determined as follows. The irradiated sample was allowed to rest in the dark for a time  $\tau$  (experimental variable). The current signal  $I \sim f(t)$  was recorded as a function of  $\tau$ .  $\Psi(\tau)$  is determined as

$$\Psi(\tau) = [I_r - I_\tau]/[I_r - I_p]$$

where  $I_r$  and  $I_p$  are the current values of dark-rested and exposed samples, respectively, immediately after illumination (current traces were chosen at  $t = t_T$ ).

Mobility measurements by the TOF method, mentioned above, are particularly important but it must be augmented by others. Xerographic techniques, initially developed to characterize electrophotographic receptors, are widely applicable to the study of amorphous thin films and photoconductive insulator thin films [18, 19, 49-52]. The high field

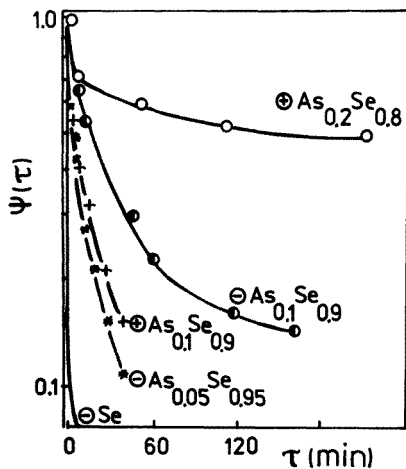


Figure 13. The relaxation function for hole (electron) metastable traps ( $T = 293$  K).

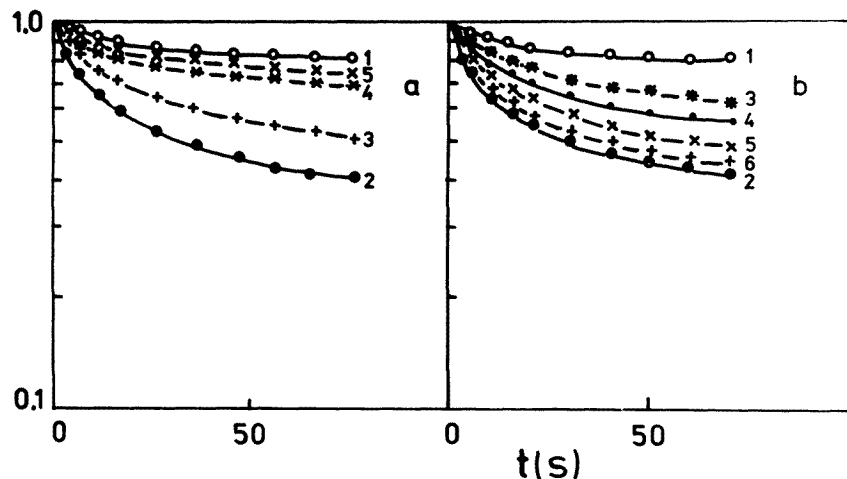


Figure 14. Surface potential dark decay in  $a\text{-As}_{0.1}\text{Se}_{0.9}$  films: (a) data 1, dark rested; data 2, exposed; data 3, 4 and 5, exposed and then dark rested for 5 min, 20 min and 30 min, respectively; (b) data 1, dark rested; data 2, exposed; data 3, 4, 5 and 6, exposed and dark rested for 30 min in the presence of a surface potential of 115 V, 170 V, 215 V and 520 V, respectively.

( $10^5\text{--}10^6$  V cm $^{-1}$ ) due to corona charging is applied to sample films, and the decay of the open-circuit surface potential is measured. This xerographic potential probe technique is a unique means to characterize electronic gap states. In particular, a map of states near midgap is determined by time-resolved analysis of the xerographic surface potential.

The illumination of amorphous films by light with energy near the optical band gap causes marked changes in the basic electrophotographic parameters, i.e. the dark discharge rate  $dU/dt$ , initial charging potential  $U_0$ , residual potential  $U_r$  and its dark-decay rate.

The parameters of dark discharge in dark-rested and exposed films are summarized

**Table 1.** Surface potential dark-decay parameters and their photoinduced changes in  $\text{As}_x\text{Se}_{1-x}$  films.

As concentration (at.%)	$dU/dt$ ( $\text{V s}^{-1}$ )	$t_{U_0/2}$ (s)	$\gamma = (dU^*/dt)/(dU/dt)$	$\Delta U/U_0$
0	$6.7 \times 10^{-2}$	276	1.06	0.30
2	$9.7 \times 10^{-2}$	150	1.20	—
5	$1.4 \times 10^{-1}$	138	1.33	—
8	$9.3 \times 10^{-1}$	19	1.61	—
10	1.22	17	2.3	—
15	1.12	18	2.5	0.50
20	1.4	15	1.9	0.52

in table 1. Here  $t_{U_0/2}$  is the half-decay time,  $\Delta U/U_0 = (U_0 - U_0^*)/(U_0)$  is the relative change in the initial charging potential (parameters of illuminated samples are indicated by an asterisk).

It is interesting to note that the time evolution of the dark-decay kinetics of the surface potential after photoexcitation is nearly the same as that observed for photocurrent transients in TOF experiments [49]. An increasing dark adaptation time, i.e. the dark-resting time of an exposed film before charging it to a certain potential and recording the potential decay, causes a reduction in the observable photoinduced changes.

The photoinduced effects are influenced by electric fields. Figure 14 clearly illustrates that the photoinduced change in the dark discharge rate may successfully be ‘frozen in’ by applying an electric field  $E = 3 \times 10^5 \text{ V cm}^{-1}$  immediately after light exposure.

The features observed in the dark-decay study can be accounted for by a depletion discharge model [50, 51]. So, the bulk process driving dark decay is emission and sweep-out of holes from states near midgap, leading to progressive formation of negative space charge. The rise in dark discharge rate and the shift of the depletion time  $t_d$  by illumination may be due to an enhanced thermal generation of holes from deep centres. From the temperature dependence of  $t_d$  it is estimated that the emitting sites are located 0.8–0.9 eV above the valence band mobility edge.

For the films under examination the residual voltage  $U_r$  increases with exposure. For example, previous photoexcitation leads to an increase in  $U_{r_1}$  (first cycle residual voltage) for Se up to 3.7 V caused by a decrease in  $\mu\tau_L$  to  $1.3 \times 10^{-7} \text{ cm}^2 \text{ V}^{-1}$ . Taking into account the invariance of  $\mu^e = 4.9 \times 10^{-3} \text{ cm}^2 \text{ V}^{-1} \text{ s}^{-1}$  with light exposure it is obvious that the lifetime reduction (from  $5.4 \times 10^{-5}$  to  $2.6 \times 10^{-5} \text{ s}$ ) is the only reason for the photoinduced change.

During the continuous repetition of xerographic cycles, the residual voltage  $U_{r_n}$  at the  $n$ th cycle was found to have the typical behaviour shown in figure 15(a). The saturation residual potential  $U_{r_s}$  provides [18, 19] a measure of the density of uniformly trapped carriers:

$$U_{r_s} = Ned^2/2\epsilon$$

where  $\epsilon$  is the dielectric constant. An increase in  $U_{r_s}$  in pre-exposed films indicates photoenhanced accumulation of charge at deep centres. We obtain  $N \approx 10^{15} \text{ cm}^{-3}$  and  $N^* \approx 4 \times 10^{15} \text{ cm}^{-3}$  for dark-rested and pre-exposed  $\text{As}_{0.1}\text{Se}_{0.9}$  films, respectively.

The residual potential decays to zero. This process is controlled by the spectrum of trap release times. The trap energies can be deduced from an analysis of isothermal residual

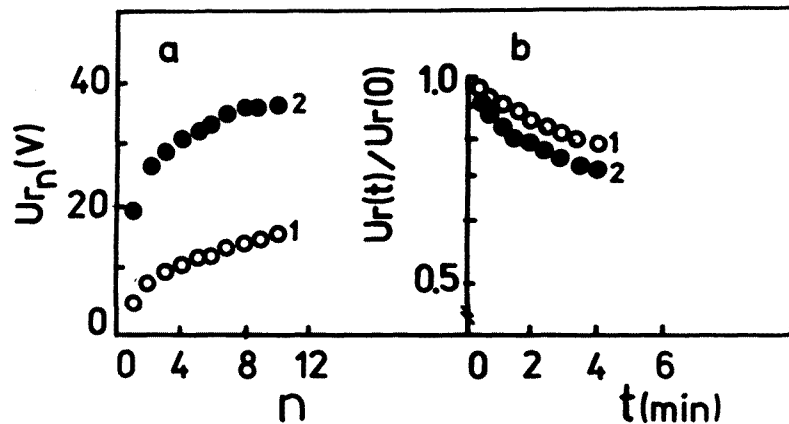


**Figure 15.** The build-up in the residual voltage with (a) number of xerographic cycles and (b) isothermal room-temperature relaxation of saturated residual voltage in dark-rested (data 1) and exposed (data 2) a-As<sub>0.02</sub>Se<sub>0.98</sub> films.

potential decay curves using

$$U_{r_s} = \sum_i C_i \exp\left(\frac{-t}{\tau_i}\right)$$

where  $\tau_i^{-1} = \nu_i \exp[-E_i/kT]$  is the release time from the  $i$ th trap,  $\nu_i$  is the frequency factor and  $E_i$  is the trap depth. We find that deep levels in amorphous selenium reside at  $E_i^h = 0.85$  eV and  $E_i^e = 1.0$  eV for holes and electrons, respectively. Their depth becomes somewhat shallower with addition of As, e.g.  $E_i^h = 0.80$  eV and  $E_i^e = 0.90$  eV in As<sub>0.1</sub>Se<sub>0.9</sub>. The more rapid decay of the residual voltage  $U_{r_s}^*$  in pre-illuminated films relative to dark-rested film (figure 15(b)) indicates a slight decrease in the depth of those states. A comparison of room-temperature recovery in TOF and xerographic measurements demonstrates that relaxation of deep metastable centres in exposed films occurs on the same time scale. In other words, the deep gap centres which control the xerographic dark decay and residual voltage are, like the trapping centres discussed in TOF experiments, characteristically metastable.

Band-gap light can, in principle, have two distinct effects on the electronic structure of the mobility gap. Band-gap light can either introduce (generate) new localized states or initiate conversion of traps of small cross section to traps of larger cross section [19]. Consequently, the latter become accessible in deep-level spectroscopy only after irradiation. In that sense we may also consider such converted localized states as ‘new’ localized states (created by irradiation).

## 5. Discussion

The irreversible structural changes which occur in the conventionally prepared (slowly deposited) thin films upon optical illumination can be understood in terms of the same mechanism as described in [5, 23–27]. These changes are associated with a photopolymerization of As<sub>4</sub>S<sub>4</sub> and S<sub>2</sub> or similar molecular species. The resultant structure formed after such transformation is a three-dimensional network with nearly restored

chemical ordering.

The rapid deposition, as indicated from the present Raman data, significantly enhances compositional as well as structural disorder in amorphous samples compared with samples of stoichiometric composition. An increase in As concentration leads to a condensation of  $\text{As}_4\text{S}_3$  and some other As-rich molecular species; a disordered molecular solid is obtained. These As-rich compositions are unstable, and presumable phase separation occurs upon thermal annealing and light irradiation. Without going into the further details of these irreversible effects in rapidly deposited films, it can be said that irreversible photoinduced structural changes in conventionally prepared amorphous films are quite different from a phenomenological point of view and also with respect to their origin.

We next discuss experimental investigations on reversible photoinduced effects in previously annealed films. Two sensitive experimental techniques, namely nuclear quadrupole resonance spectroscopy [53] and Raman spectroscopy (see present Raman data), failed to detect any gross changes in the local bonding configuration. However, other structural probes, namely infrared absorption [28] and differential anomalous x-ray scattering [54], show that small changes do occur under illumination. A mechanism proposed by Elliott [4] to account for the light-induced changes in the structure depicts photodarkening in chalcogenide glasses in terms of intra-molecular and inter-molecular bond breaking and bond weakening. According to this model, the increase in homopolar bonding would have to be substantially larger (about 7% for  $\text{As}_2\text{S}_3$ ) than measured (from 1.5 to 2.0%) to account for the observed changes. Our principal conclusions are similar to those of Elliott [4], Yang *et al* [29] and Zhou *et al* [54]. We agree that, although some local configurations may contribute to photodarkening, the phenomenon cannot be explained in terms of these local changes alone.

The most significant photostructural change observed using the Raman scattering technique is in the region of the low-frequency or Boson peak at a wavelength of about  $25 \text{ cm}^{-1}$ . This Raman peak is accounted for as signifying certain medium-range order in an amorphous structure [55–57]. The position and the intensity of the peak can be used to estimate the structural correlation length  $R_c$  ( $\sim (\omega_{\text{max}}/V)^{-1}$ , where  $\omega_{\text{max}}$  is the frequency of the peak maximum and  $V$  is the sound velocity) and to characterize the degree of structural ordering. The structural correlation length has generally been associated with the dimensions of some cluster-like structures. For a- $\text{As}_2\text{S}_3$ , the  $R_c$ -value is about 7.6 Å. The clusters are possibly in the form of linkages of pyramids. In spite of the absence of final conclusions on the nature of the low-energy excitations in disordered solids it is obvious that differences between the boson peak in the annealed and photodarkened state are due to changes in medium-range order. A decrease in the peak height and a shift to higher  $\omega$ -values may be attributed to an increase in structural randomness. This is consistent with an increase in structural disorder under illumination detected in XAFS spectra [29, 58] and in x-ray scattering [2]. Thus our experimental results on Raman scattering agree qualitatively with the hypothesis that photodarkening is a photostructural change and is the result of changes in medium-range order (e.g. weakly linked  $\text{AsS}_3$  pyramids move with respect to each other as proposed in [6]). This mechanism does not involve covalent bond breaking.

Let us consider the role played by electronic gap states in photoinduced changes. We speculate that the mechanism of photodarkening consists of the following. Band-gap radiation initially causes excitation of the electron subsystem. The incident photon creates electron–hole pairs. These photogenerated electrons and holes may be assumed to be initially in free (mobile) states in the bands. Part of the excess carrier energy is transferred into heat. In the first place, the photogenerated electrons and holes are both rapidly trapped at the defect states. These defects cause local levels in the energy gap and

affect the physical properties (i.e. optical, dielectric and electrical). We identify such gap centres as arising from charged native defects such as  $C_3^+$  and  $C_1^-$  in pure selenium. After trapping, the lattice surrounding the defect distorts. The resulting local relaxation evidently stabilizes the trapped carriers, which must then produce excess defect centres. The latter efficiently affect the photoconductivity and transport properties of amorphous chalcogenides (e.g. enhance carrier trapping as shown by our TOF and xerographic experiments). Since the metastable states are local potential minima after the relaxations, a potential barrier must exist, retarding the transition to the initial state. Annealing of the material removes the new defects and restores the original balance. Therefore, the picture that we used is that normally empty precursor states (in other words, states that exist in quasi-equilibrium before the system is illuminated) become filled during illumination. As a result of the non-equilibrium occupation of electronic gap states, the physical properties (optical and photoelectronic) are altered.

With regard to the low-temperature data, we suggest that there exists a kind of defect which is closely related to this component of photodarkening. Indeed, the TSC truly reflects the release from some localized states. TSC and grating experiments provide strong evidence that carrier trapping at these states is the primary effect whereas the structural change (and concomitant change in the absorption coefficient and refractive index) is the secondary effect. In a-As<sub>0.5</sub>Se<sub>0.5</sub>, the corresponding activation energy is about 0.4 eV. Since the TOF measurements show that the only mobile carriers in As<sub>0.5</sub>Se<sub>0.5</sub> are positive holes [39], the above trapping centres are most likely to act as hole traps.

At room temperature, deep trapping of injected carriers (of both sign) is enhanced in photodarkened samples. Such illumination can cause an increase in the deeply trapped space-charge density induced by repetitive TOF cycling but has no appreciable effect on the drift mobility value. These observations support the conclusion that the main influence of band-gap illumination on As<sub>x</sub>Se<sub>1-x</sub> alloys is the generation of deep states which act as efficient hole ( $E_i^h = 0.8\text{--}0.9$  eV) and electron ( $E_i^e = 0.9\text{--}1.0$  eV) traps.

It is of interest to point out that the 'memory' effect (the persistence of light-induced metastabilities) becomes appreciably prolonged with increasing As content (see figure 13). These investigations show the importance of the arsenic-related defects in photoinduced changes. Even without a detailed understanding of the microscopic mechanism, the relationship between the metastable trap lifetime and chemical composition can be interpreted in terms of As-induced deep centres. We suggest that the addition of As to a-Se increases the integrated number of deep traps which are predisposed to become photodarkened sites. TOF experiments, i.e. the absence of electron drift as the As content becomes appreciable ( $x > 0.2$ ) [44, 59, 60], indicate that As introduces a sufficient concentration of deep electron traps to eliminate electron transport. The network modifications (induced by threefold-coordinated As atoms) and the change in the mobility gap structure may, of course, be related.

Finally, the results for As<sub>x</sub>Se<sub>1-x</sub> tempt us to assume that the observed photoenhanced deep trapping is a universal property in amorphous chalcogenides subjected to band-gap light.

## 6. Concluding remarks

In this paper the influence of band-gap irradiation on the atomic and mobility gap structure was studied with the aim of providing insight into the mechanism of light-induced changes. The major experimental findings of these studies may be summarized as follows.

(1) For the case of amorphous arsenic–sulphur alloys, a very high evaporation rate induces the development of a tendency to microcrystallite formation. Heat or light treatment further enhances the crystallization processes. The irreversible changes observed in the Raman spectra of slowly deposited films are interpreted in terms of the photopolymerization mechanism.

(2) Our study has shown that, although reversible photodarkening in  $\text{As}_2\text{S}_3$  films is strongly pronounced, the local structural changes are relatively insignificant. The most significant structural changes occur in the medium-range order.

(3) We have identified systematic photoinduced changes in electronic transport and trapping with changes in localized defect states. For the case of ambipolar  $\text{As}_x\text{Se}_{1-x}$  ( $x \leq 0.2$ ), light-induced variation in the respective densities of hole and electron deep traps is demonstrated.

(4) The TSC, TOF and xerographic experiments seem to indicate that carrier trapping at defect states is essential to the photodarkening phenomenon.

### Acknowledgments

Many thanks are due particularly to my close collaborators Ivan Mikhalko and Alexandra Levkulich. This work has benefited from the extensive participation of Alexander Mateleshko and Andrej Baganich.

### References

- [1] De Neufville J P 1975 *Optical Properties of Solids—New Developments* ed B O Seraphin (Amsterdam: North-Holland) p 437
- [2] Tanaka K 1990 *Rev. Solid State Sci.* **2-3** 644
- [3] Lyubin V M 1985 *Physics of Disordered Materials* ed D Adler, M Kastner and H Fritzsche (New York: Plenum) p 673
- [4] Elliott S R 1986 *J. Non-Cryst. Solids* **81** 71
- [5] Owen A E, Firth A P and Ewen P J S 1985 *Phil. Mag. B* **52** 347
- [6] Pfeiffer G, Paesler M A and Agarwal S C 1991 *J. Non-Cryst. Solids* **130** 111
- [7] Berkes J S, Ing S W and Hillegas W J 1971 *J. Appl. Phys.* **42** 4908
- [8] Kolomiets B T and Lyubin V M 1978 *Mater. Res. Bull.* **13** 1343
- [9] Kolomiets B T, Lyubin V M and Shilo V P 1978 *Fiz. Khim. Stjekla* **11** 351
- [10] Kolomiets B T, Lantratova S S, Lyubin V M and Shilo V P 1979 *Fiz. Tverd. Tela* **21** 1028
- [11] Hamanaka H, Tanaka K and Iizima A 1977 *Solid State Commun.* **23** 63
- [12] Averjanov V L, Kolomiets B T, Lyubin V M and Taguyardzhanov M A 1977 *Proc. 7th Int. Conf. on Amorphous and Liquid Semiconductors* (Bristol: Institute of Physics) p 802
- [13] Kikineshi A A, Mikla V I, Semak D G and Pinzenik V P 1978 *Ukr. Fiz. Zh.* **23** 63
- [14] Mikla V I, Semak D G and Kikineshi A A 1980 *Ukr. Fiz. Zh.* **25** 2021
- [15] Baganich A A, Mikla V I, Semak D G, Sokolov A P and Shebanin A P 1991 *Phys. Status Solidi b* **166** 297
- [16] Spear W E 1969 *J. Non-Cryst. Solids* **1** 197
- [17] Pfister G and Scher H 1978 *Adv. Phys.* **27** 747
- [18] Abkowitz M and Enck R C 1982 *Phys. Rev. B* **25** 2567
- [19] Abkowitz M and Enck R C 1983 *Phys. Rev. B* **27** 7402
- [20] Mikla V I, Vysochanski Yu M, Kikineshi A A, Semak D G and Stefanovich V A 1983 *Izv. Vuzov (Fiz.)* **11** 73 (Engl. Transl. 1983 *Sov. Phys.* **11** 58)
- [21] Zhdanov V G and Malinovskij V K 1979 *Preprint* 106 (Novosibirsk: Institute of Automation and Electrometry) p 27
- [22] Borisova Z U 1972 *Chemistry of Vitreous Semiconductors* (Leningrad: Izdatel' stvo Leningradskogo Universiteta) (in Russian) p 271
- [23] Solin S A and Papatheodorou G N 1977 *Phys. Rev. B* **15** 2084
- [24] Nemanich R J, Connell G A N, Hayes T M and Street R A 1978 *Phys. Rev. B* **12** 6900

- [25] Slade N L and Zallen R 1979 *Solid State Commun.* **30** 357
- [26] Ewen P J S, Sik M I and Owen A E 1980 *Solid State Commun.* **33** 1067
- [27] Strom U and Martin T P 1979 *Solid State Commun.* **29** 527
- [28] Shpotyuk O I, Kornelyuk V N and Jaskovec I I 1990 *Zh. Prikl. Spektrosk.* **52** 602
- [29] Yang S Y, Paesler M A and Sayers D E 1987 *Phys. Rev. B* **36** 9160
- [30] Turjanica I I, Kikineshi A A and Semak D G 1979 *Ukr. Fiz. Zh.* **24** 543
- [31] Tanaka K, Gohda S and Odajima A 1985 *Solid State Commun.* **56** 899
- [32] Bertoluzza A, Fagnano C, Monti P and Semerano A 1978 *J. Non-Cryst. Solids* **29** 49
- [33] Yang C Y, Sayers D E and Paesler M A 1987 *Phys. Rev. B* **36** 8122
- [34] Mikla V I, Rubish V M and Zabedovskij B A 1990 *Proc. Int. Daylighting Conf. 'Daylighting-90'* (Moscow: CIE) p 61
- [35] Tanaka K 1975 *Appl. Phys. Lett.* **26** 243
- [36] Frumar M, Firth A P and Owen A E 1984 *Phil. Mag.* **50** 453
- [37] Mikla V I, Semak D G, Stefonovich V A and Slivka V Yu 1987 *Fiz. Khim. Stjekla* **13** 808
- [38] Semak D G, Mikla V I, Mikhalko I P, Stefanovich V A, Slivka V Yu and Visochanskij Yu M 1984 *Fiz. Tverd. Tela* **26** 3210 (Engl. Transl. 1984 *Sov. Phys.-Solid State* **26** 1934)
- [39] Mikla V I 1984 *PhD Thesis* Odessa State University
- [40] Vlasov V I, Mikla V I, Mikhalko I P 1977 *Structure and Physical Properties of Thin Films* ed D V Chepur (Uzhgorod: Patent) p 624
- [41] Agarwal S C and Fritzsch H 1974 *Phys. Rev. B* **10** 4351
- [42] Orenstein J, Kastner M and Vaninov V 1982 *Phil. Mag. B* **46** 23
- [43] Arnoldussen T C, Bube R H, Fagen E A and Holmber S H 1972 *J. Appl. Phys.* **43** 1798
- [44] Mott N F and Davis E A 1982 *Electronic Processes in Non-Crystalline Materials* 2nd edn (Moscow: Mir) (Russian Transl.)
- [45] Street R A 1978 *Phys. Rev. B* **17** 3984
- [46] Tanaka K and Odajima A 1982 *Solid State Commun.* **43** 961
- [47] Averjanov V L, Kolobov A V, Kolomets B T and Lyubin V M 1980 *Phys. Status Solidi a* **57** 81
- [48] Garlick G P and Gibson A F 1948 *Proc. Phys. Soc.* **60** 574
- [49] Mikla V I, Semak D G, Mateleshko A V and Baganich A A 1990 *Phys. Status Solidi a* **117** 241
- [50] Melnyk A R 1980 *J. Non-Cryst. Solids* **35-36** 837
- [51] Abkowitz M 1987 *J. Non-Cryst. Solids* **97-98** 1163
- [52] Kasap S O 1991 *Handbook of Imaging Materials* ed A S Diamond (New York: Marcel Dekker) p 329
- [53] Treacy D J, Taylor P C and Klein P B 1979 *Solid State Commun.* **32** 423
- [54] Zhou W, Sayers D E, Paesler M A, Bouchet-Fabre B, Ma Q and Raoux D 1993 *Phys. Rev. B* **47** 686
- [55] Martin A J and Brenig W 1974 *Phys. Status Solidi b* **63** 163
- [56] Nemanich R J 1977 *Phys. Rev. B* **16** 1655
- [57] Malinovsky V K and Sokolov A P 1986 *Solid State Commun.* **57** 757
- [58] Gladden L F, Elliott S R and Greaves G N 1988 *J. Non-Cryst. Solids* **106** 189
- [59] Marshall J M 1974 *Phys. Status Solidi a* **25** 419
- [60] Owen A E and Spear W E 1976 *Phys. Chem. Glasses* **17** 174